

The FRD3 Citrate Effluxer Promotes Iron Nutrition between Symplastically Disconnected Tissues throughout *Arabidopsis* Development

Hannetz Roschttardt^{1,2}, Mathilde Séguéla-Arnaud^{1,3}, Jean-François Briat, Grégory Vert, and Catherine Curie⁴

Biochimie et Physiologie Moléculaire des Plantes, Centre National de la Recherche Scientifique, UMR 5004/Institut National de la Recherche Agronomique/SupAgro/Université Montpellier 2, F-34060 Montpellier Cedex 2, France

We present data supporting a general role for FERRIC REDUCTASE DEFECTIVE3 (FRD3), an efflux transporter of the efficient iron chelator citrate, in maintaining iron homeostasis throughout plant development. In addition to its well-known expression in root, we show that *FRD3* is strongly expressed in *Arabidopsis thaliana* seed and flower. Consistently, *frd3* loss-of-function mutants are defective in early germination and are almost completely sterile, both defects being rescued by iron and/or citrate supply. The *frd3* fertility defect is caused by pollen abortion and is associated with the male gametophytic expression of *FRD3*. Iron imaging shows the presence of important deposits of iron on the surface of aborted pollen grains. This points to a role for *FRD3* and citrate in proper iron nutrition of embryo and pollen. Based on the findings that iron acquisition in embryo, leaf, and pollen depends on *FRD3*, we propose that *FRD3* mediated-citrate release in the apoplastic space represents an important process by which efficient iron nutrition is achieved between adjacent tissues lacking symplastic connections. These results reveal a physiological role for citrate in the apoplastic transport of iron throughout development, and provide a general model for multicellular organisms in the cell-to-cell transport of iron involving extracellular circulation.

INTRODUCTION

Iron is essential for a plethora of cellular functions. In plants, its availability is known to affect developmental programs such as root morphogenesis (Schmidt, 1999) and flower development and color (Takahashi et al., 2003; Momonoi et al., 2009). Iron entry in the biosphere is often limited by its solubility in the soil, despite its great abundance. In particular, Fe^{3+} ions precipitate in alkaline soils, thereby preventing their extraction by plant roots. Symptoms of iron shortage in plants include chlorosis and poor growth due to the impairment of numerous metabolic pathways that require iron-containing proteins. To cope with iron deficiency, plants have developed physiological and molecular strategies that increase iron mobilization in the rhizosphere and enable high-affinity iron uptake. In *Arabidopsis thaliana*, these include (1) a modification of the root architecture to increase foraging capacity, (2) the acidification of the root vicinity by rhizodermic cells through the proton ATPase *AHA2* (Santi and Schmidt, 2009) and to the extrusion of organic acids, (3) the reduction of Fe^{3+} in Fe^{2+} by a ferric-chelate reductase encoded

by the *FERRIC REDUCTASE OXIDASE2* (*FRO2*) gene (Robinson et al., 1999), and (4) the uptake of Fe^{2+} by the metal transporter IRON REGULATED TRANSPORTER1 (*IRT1*) (Eide et al., 1996; Henriques et al., 2002; Varotto et al., 2002; Vert et al., 2002). As *IRT1* displays a broad selectivity for metal ions (Eide et al., 1996), it is also responsible for the perverse entry of heavy metals in iron-starved plants (Vert et al., 2002). Expression of the *IRT1* and *FRO2* genes, which occurs specifically in root epidermal cells of iron-deficient plants, is mostly controlled at the transcriptional level (Connolly et al., 2002; Vert et al., 2002, 2003) and involves the basic HELIX LOOP HELIX transcription factor Fe-DEFICIENCY INDUCED FACTOR1, itself upregulated by iron deficiency (Colangelo and Guerinot, 2004; Jakoby et al., 2004; Yuan et al., 2005).

Because free ionic iron can cause cell damage by catalyzing the production of highly toxic reactive oxygen species, iron is always found bound to its target metalloproteins or chelated to organic or mineral ligands. Citrate is likely an important ligand of iron in animals and plants, in particular, in the extracellular fluids. In the brain interstitium where citrate is released in large amount by astrocytes, part of the nontransferrin-bound iron pool that circulates might be complexed with citrate because neurons have been shown to take up Fe-citrate (reviewed in Moos et al., 2007). In the xylem sap of many plant species, iron has been thought to circulate as Fe-citrate. Citrate concentration is indeed markedly increased by iron starvation in xylem exudates (Brown, 1966; López-Millán et al., 2000), and the acidic pH of this apoplastic fluid is compatible with the stability of the Fe-citrate complex. Only recently, however, has the presence of Fe-citrate complexes, in the form of tri-Fe(III) tri-citrate and di-Fe(III) di-citrate, been detected in xylem exudates of tomato plants (Rellán-Alvarez et al., 2010).


¹ These authors contributed equally to this work.

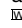
² Current address: Department of Botany, University of Wisconsin, B122 Birge Hall, 430 Lincoln Dr., Madison, WI 53706.

³ Current address: John Innes Center, Norwich Research Park, Colney, Norwich NR4 7UH, United Kingdom.

⁴ Address correspondence to curie@supagro.inra.fr.

The author responsible for distribution of materials integral to the findings presented in this article in accordance with the policy described in the Instructions for Authors (www.plantcell.org) is: Catherine Curie (curie@supagro.inra.fr).

 Some figures in this article are displayed in color online but in black and white in the print edition.

 Online version contains Web-only data.

www.plantcell.org/cgi/doi/10.1105/tpc.111.088088

Multidrug and toxic compound extrusion (MATE) transporters are involved in the efflux of xenobiotics and metabolites from cells in prokaryotes and eukaryotes (reviewed in Omote et al., 2006). The number of MATE-type transporters is very large in plants compared with bacteria and animals. The *Arabidopsis* genome encodes 58 MATE transporters, which suggests that plants can efflux a large number of metabolites (Yazaki, 2005). Thus far, only a few plant MATEs have been functionally characterized. A number of MATEs transport endogenous molecules, such as pigments, in the vacuole. *Arabidopsis* TRANSPARENT TESTA 12 and *Medicago truncatula* MATE1 transport precursors for proanthocyanidin biosynthesis in the vacuole of seed coat cells (Debeaujon et al., 2001; Marinova et al., 2007; Zhao and Dixon, 2009), whereas in grapevine berries, *AnthoMATE1* and *AnthoMATE3* likely transport acylated anthocyanins in the vacuole (Gomez et al., 2009). Other MATE members detoxify endogenous molecules, xenobiotics, and toxic elements by efflux into the apoplastic space. *Arabidopsis thaliana* detoxification1 was shown to mediate efflux of plant-derived alkaloids, antibiotics, and Cd²⁺ (Li et al., 2002). Moreover, as shown in many plant species, aluminum tolerance is conferred by MATE-mediated citrate efflux in the rhizosphere (Li et al., 2002; Furukawa et al., 2007; Liu et al., 2009; Maron et al., 2010).

Arabidopsis FERRIC REDUCTASE DEFECTIVE3 (FRD3) and its ortholog in rice (*Oryza sativa*), Os FRDL1, are plasma membrane citrate efflux transporters and represent important components of the iron homeostasis machinery (Rogers and Guerinot, 2002; Green and Rogers, 2004; Durrett et al., 2007; Yokosho et al., 2009). The first mutant allele of *FRD3* was isolated as a manganese accumulator plant of *Arabidopsis*, hence was designated *man1* (Delhaize, 1996). *man1* was described as a chlorotic and dwarf mutant that contains an increased concentration of iron in the root and displays a constitutive root ferric-chelate reductase activity (Delhaize, 1996). Two additional alleles, *frd3-1* and *frd3-2*, were isolated in a screen for *Arabidopsis* ethyl methanesulfonate (EMS)-mutagenized mutants with constitutive root ferric-chelate reductase activity (Rogers and Guerinot, 2002). In *Arabidopsis frd3* and rice *frd1* knockout mutants, the expression of iron deficiency-induced genes is high regardless of the iron status (Rogers and Guerinot, 2002; Yokosho et al., 2009). Expression analysis of *FRD3* and Os *FRDL1* genes indicated that their transcript accumulation is only slightly modulated by iron nutrition (Rogers and Guerinot, 2002; Yokosho et al., 2009). In addition, *FRD3* promoter activity and Os FRDL1 protein are localized to the root pericycle (Green and Rogers, 2004; Yokosho et al., 2009). Both the *Arabidopsis* and rice proteins mediate citrate efflux when produced in *Xenopus laevis* oocytes (Durrett et al., 2007; Yokosho et al., 2009). Iron staining in the root revealed a strong accumulation of iron in the stele of the *Arabidopsis* and rice mutants. Consistent with the iron starvation symptoms in leaves (Green and Rogers, 2004; Durrett et al., 2007; Yokosho et al., 2009), citrate and iron concentrations were reduced in xylem exudates. Therefore, it was proposed that the function of FRD3/Os FRDL1 is to release citrate into the root xylem, which would in turn be required for efficient translocation of iron to the shoot. Although protoplasts prepared from *frd3* leaves display decreased iron content (Green and Rogers, 2004), total leaf iron is similar in *frd3* and wild-type plants (Delhaize, 1996). Thus, in

addition to promoting root-to-shoot circulation of iron in the xylem sap, citrate might represent an important ligand for the passage of iron from the apoplast to the symplast in leaf.

In this article, we report that a genetic screen designed to isolate regulatory mutants of iron homeostasis enabled us to isolate a new *frd3* allele. It prompted us to clarify the role that FRD3, and by extension, citrate, play in iron allocation and partitioning between apoplast and symplast, and how FRD3 impacts plant development at different stages. We show that *FRD3* is strongly expressed in the developing embryo where it is required for efficient germination in iron-limiting conditions. We also demonstrate, using iron histochemical staining, that later in plant development, citrate released by FRD3 in the vascular tissues enables iron solubilization and circulation in the apoplast located around the vascular tissues throughout the plant, and promotes iron mobilization to the cells adjacent to the leaf veins. Finally, we observed that *frd3* mutants display a drastic fertility defect caused by an alteration of pollen development, itself resulting from shortage of soluble iron in the anther locule. Based on these data, we propose a model in which citrate efflux mediated by FRD3 allows iron solubilization in the apoplastic space separating two tissues without symplastic connections. Our results indicate that this process likely provides available iron to sustain germination of the embryo, growth of leaf mesophyll cells, and development of the pollen grains.

RESULTS

Isolation and Characterization of Two Novel *frd3* Alleles

Screening EMS-mutagenized pro $IRT1$:LUCIFERASE transgenic plants for *Arabidopsis* mutants that are unable to properly regulate *IRT1* promoter activity (see Supplemental Figure 1 online) enabled us to isolate a new *frd3* allele called *frd3-6* (Figure 1A). Several other loss-of-function alleles of *FRD3*, named *frd3-1*,

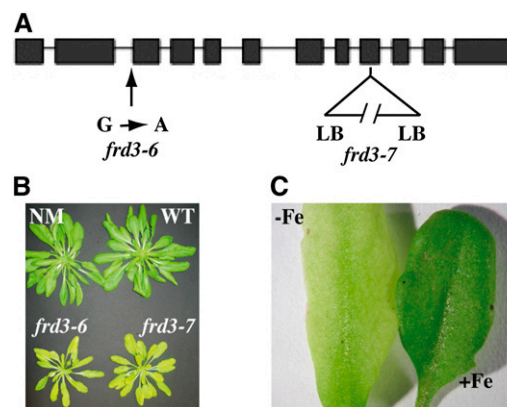


Figure 1. Phenotype of Two New Alleles of *FRD3*.

(A) Position of *frd3-6* and *frd3-7* mutations on the *FRD3* gene. LB, left border; G → A, guanine to adenine transversion.

(B) Phenotype of 7-week-old *frd3-6* and *frd3-7* mutants grown in soil. NM, nonmutagenized parental line; WT, wild type.

(C) *frd3* chlorosis is reverted by iron supply. Four-week-old *frd3-6* plants cultivated on soil were irrigated with water (–Fe) or 0.5 mM FeEDDHA (+Fe).

frd3-2, *frd3-3/man1*, and *frd3-5*, have been reported (Delhaize, 1996; Rogers and Guerinot, 2002; Lahner et al., 2003) and are shown to have iron homeostasis defects during vegetative growth. Whether the corresponding FRD3 mutant proteins harbor decreased citrate efflux activity or are completely nonfunctional is currently unknown. To explore the precise role of FRD3 in the maintenance of iron homeostasis during plant development, we collected a knockout mutant (SALK_122535), named hereafter *frd3-7*, carrying a T-DNA insertion within exon 8 (Figure 1A) that completely abolishes *FRD3* mRNA accumulation (see Supplemental Figure 1 online).

As for some of the *frd3* alleles previously described, *frd3-6* and *frd3-7* mutant plants showed smaller rosette leaves and severe chlorosis when cultivated in soil in greenhouse conditions (Figure 1B). Their chlorosis was reverted by exogenous iron supply

(Figure 1C). Consistent with the literature (Delhaize, 1996; Rogers and Guerinot, 2002; Lahner et al., 2003) and with the increased *IRT1* promoter activity in *frd3-6* (see Supplemental Figure 1 online), the level of *IRT1* and *FRO2* mRNAs was increased in *frd3-6* and *frd3-7* alleles (see Supplemental Figure 1 online).

Role of FRD3 at the Vegetative Stage

Previous reports have established that *FRD3* is expressed only in the root, and more precisely, in the pericycle and vascular cylinder (Rogers and Guerinot, 2002; Green and Rogers, 2004). We generated transgenic *Arabidopsis* plants expressing β -Glucuronidase (GUS) under the control of the *FRD3* promoter to determine the *FRD3* expression pattern at all stages in the plant's life. Histochemical analysis of GUS activity showed the

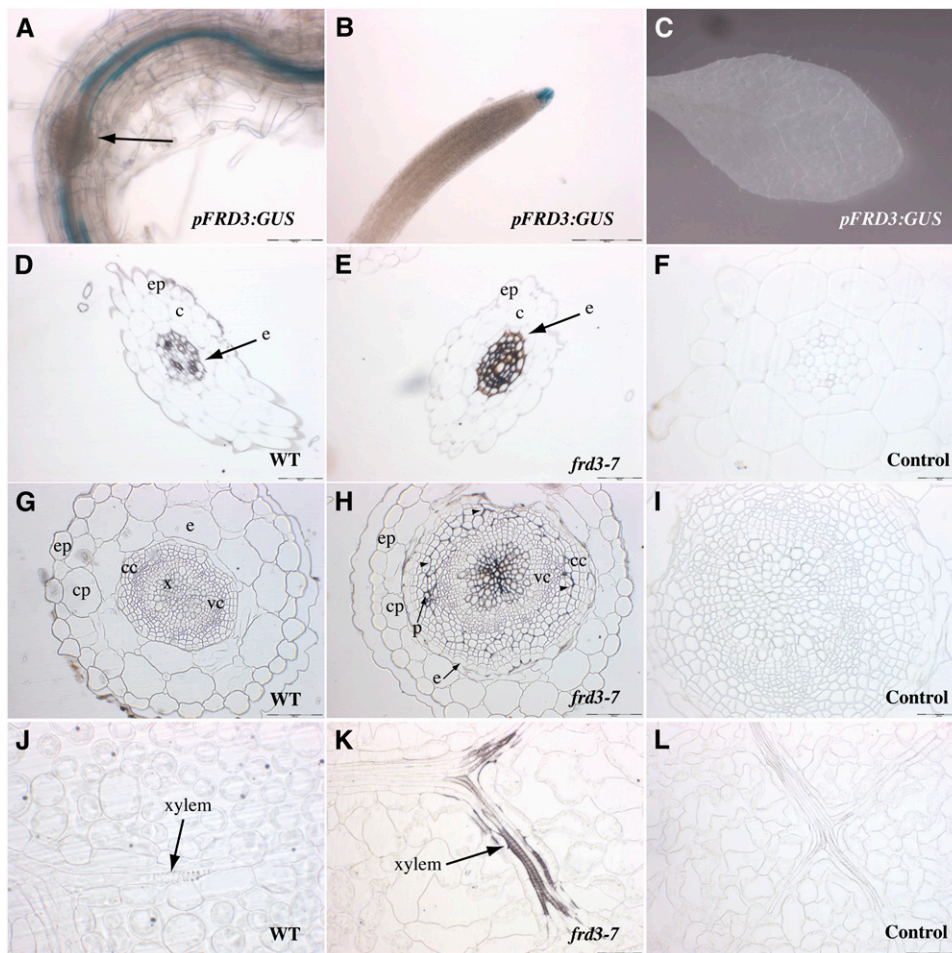


Figure 2. *FRD3* Promoter Activity in Root and Shoot, and Iron Distribution in the *frd3-7* Mutant.

(A) to (C) Histochemical GUS staining of pro*FRD3*:GUS plants from a representative transgenic line. (A) and (B) Primary root from a 1-week-old axenically grown plant in the mature zone (A) or the meristematic zone (B). The arrow in (A) shows a developing lateral root. (C) Rosette leaf of a 4-week-old soil-grown plant.

(D) to (L) Perl/DAB staining of thin sections of 4-week-old wild-type (WT; [D], [G], and [J]) or *frd3-7* plants ([E], [F], [H], [I], [K], and [L]). Roots ([D] to [F]), hypocotyl ([G] to [I]), and rosette leaves ([J] to [L]) are shown; (F), (I), and (L) are staining negative controls without Perl. c, cortex; cc, cork cambium; cp, cortex parenchyma; e, endodermis; ep, epidermis; p, phloem; vc, vascular cambium; x, xylem; arrowheads in (H) indicate the line of separation between vascular and cork cambium. Scale bars = 50 μ m in (D), (E), (I), (J), (K), and (L), 100 μ m in (A), (G), and (H), and 200 μ m in (B).

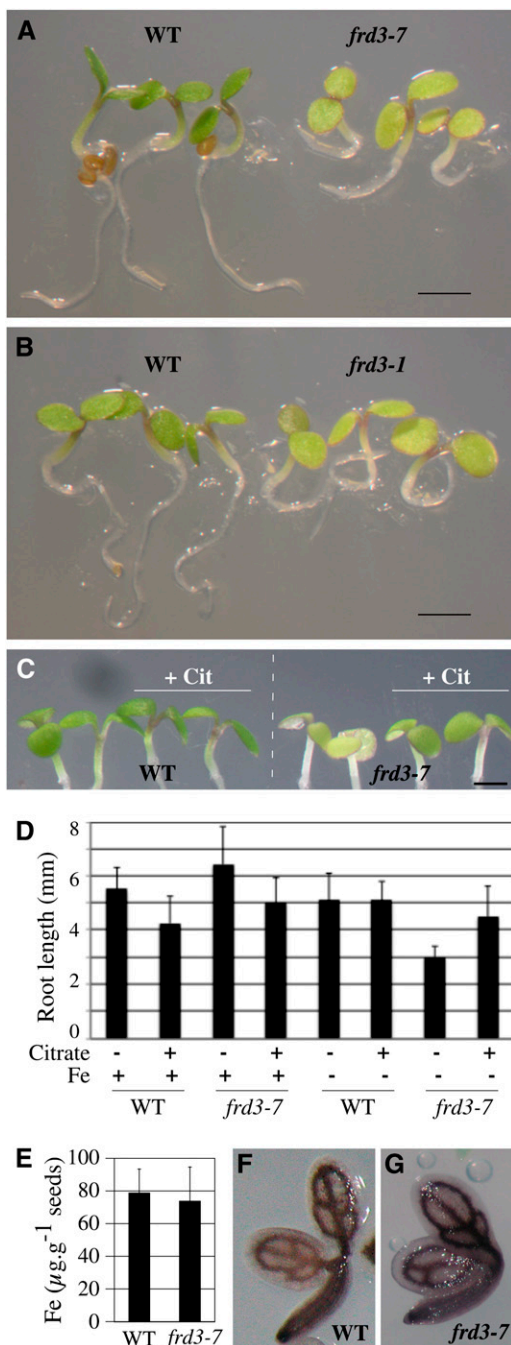


Figure 3. *FRD3* Is Required for Efficient Germination in Iron-Deficient Conditions.

(A) and **(B)** Chlorosis and reduced size of 3-d-old *frd3-7* **(A)** and *frd3-1* **(B)** seedlings grown under iron deficiency (no added iron) compared with wild-type (WT) plants.

(C) and **(D)** Citrate supplementation partially rescues the germination defect of the *frd3* mutant. Wild-type and *frd3-7* plants were grown for 3.5 d under iron sufficiency (50 µM FeEDTA, +Fe) or iron deficiency (no added iron) in the presence or absence of 3 mM Na citrate (+Cit) as indicated. Citrate treatment rescues *frd3-7* chlorosis **(C)** and root growth defect **(D)**. Scale bars = 1 mm.

presence of strong staining in roots and the absence of staining in leaves (Figures 2A and 2C). In the root, staining was found in the pericycle based on its disappearance upon lateral root formation (Figure 2A), as well as in the root cap (Figure 2B).

Previously, a strong accumulation of iron had been detected in the root vascular cylinder of the *frd3-1* mutant (Green and Rogers, 2004). To further identify the cellular compartment of iron location in the *frd3-7* root, we stained thin cross-sections of these tissues using the highly sensitive and resolutive Perls-diamino benzidine (DAB) histochemical method (Roschztartzt et al., 2009). Compared with the negative control (Figure 2F), wild-type roots displayed some deposits of iron around all the stele cells, including pericycle and vascular tissues (Figure 2D). The iron deposits were dramatically increased in *frd3-7* roots (Figure 2E). Iron accumulation was typically observed outlining the cells—but not within the cells—of the entire stele region delimited by the casparian strip (Figure 2E). This indicates that accumulation of iron in *frd3-7* is restricted to the apoplast, in a region of the root central cylinder enclosed within the casparian strip. This apoplastic iron deposition associated with the decrease of circulating iron and citrate in the xylem sap of the *frd3* mutant (see Supplemental Figure 2 online and Durrett et al., 2007) is consistent with citrate being required to solubilize apoplastic iron in the central cylinder.

We then tested whether similar iron precipitation occurred in other organs. In the hypocotyl, we observed elevated iron levels in the vascular cambium of *frd3-7* compared with wild-type plants (Figure 2G), with strong Perls/DAB staining in the apoplast surrounding the xylem vessels (Figure 2H). The intensity of the staining tended to decrease in the peripheral vessels. Iron deposits were also detected around the secondary phloem vessels, as well as in the apoplastic space, forming a separation line between vascular and cork cambium. Because the cork cambium is generated by division of the pericycle layer, the presence of iron in this region is reminiscent of the root pattern (Figure 2H). The accumulation of iron in the hypocotyl of *frd3-7* is likely an indirect consequence of the lack of *FRD3* in the root because the *FRD3* promoter is not active in the hypocotyl except very early in development (see below).

The *frd3* mutant is chlorotic despite an iron content in leaves that is, depending on the growth conditions, similar to or higher than that of wild-type plants (Delhaize, 1996; Rogers and Gueriot, 2002; Lahner et al., 2003). As for the hypocotyl, no detectable GUS activity driven by *FRD3* promoter was detected in leaves (Figure 2C). To pinpoint the cause of the leaf chlorosis in *frd3*, we performed Perls-DAB histochemical analysis on *frd3-7* leaf cross-sections. Strong iron staining was detected in *frd3-7* vasculature, particularly around the xylem vessels (Figure 2K), whereas no staining was observed in the vasculature of wild-type plants (Figure 2J). Conversely, the amount of symplastic iron in mesophyll cells decreased in *frd3-7* compared with wild type (Figures 2J and 2K). This result establishes that in the absence of

(E) Iron content in wild-type and *frd3-7* seeds. Error bars = SD.

(F) and **(G)** Iron localization in wild-type **(F)** and *frd3-7* **(G)** dry seed embryos assayed by Perls/DAB histochemical staining.

FRD3 activity, iron precipitates in the vascular cells of the leaf and fails to enter the mesophyll, thus inducing leaf chlorosis.

Collectively, these results show that in the absence of FRD3 in the root, deposition of iron likely due to iron precipitation occurs in the apoplast of vascular tissues throughout the vegetative parts of the plant. This result further supports a role for citrate efflux in solubilization of the apoplastic iron pool stored around the vascular tissues, and points to an important function of citrate in the process of iron unloading from xylem vessels and its subsequent entry into the symplast of leaf cells.

Role of FRD3 during Germination

The *frd3-7* mutant showed slow root growth and chlorotic cotyledons as early as 1 to 3 d after germination, specifically in conditions of iron deficiency (Figures 3A and 3D). Identical defects were observed for *frd3-1* (Figure 3B) and *frd3-6* (see Supplemental Figure 3 online) alleles. This observation revealed that in addition to its function in iron mobilization in xylem, FRD3 is also necessary for early development. Iron supplementation fully rescued the *frd3-7* phenotype, increasing by over twofold its root growth (Figure 3D), thus strongly suggesting that germination of the *frd3* mutant is limited by iron availability. However, this phenotype is neither explained by a decrease of iron in the seed (Figure 3E), nor by a defect of iron distribution as revealed by Perls/DAB staining of wild-type and *frd3-7* dry seed embryos (Figures 3F and 3G). To test the hypothesis that it is the absence of citrate excretion that causes improper iron nutrition of *frd3* embryos, germination of *frd3-7* was performed in the presence of citrate. This treatment significantly rescued the phenotype of *frd3-7* plants, which showed greening of the cotyledons (Figure 3C, + Cit) and higher root growth (Figure 3D) under iron deficiency. This result clearly supports the idea that citrate efflux by

FRD3 contributes to iron nutrition of the embryo during the early stage of germination. GUS histochemical analysis of ProFRD3:GUS lines showed that the *FRD3* promoter is active throughout the embryo, during its maturation prior (Figures 4A and B), and after (Figure 4C) seed desiccation. This is consistent with the elevated *FRD3* mRNA accumulation measured in siliques (see Supplemental Figure 4 online). Cross-sections of the embryo at the dry seed stage showed staining of all the tissues, with a more pronounced coloration in the protodermis layer (Figure 4G). During the early stages of germination, GUS staining was restricted to the cotyledons, and to a lower extent, to the hypocotyl (Figures 4D and 4E). At the emergence of the first pair of leaves, GUS staining faded away in the cotyledons and appeared in the root stele (Figures 4F and 4I). Interestingly, the envelope of the seed showed strong GUS staining in the aleurone layer (Figure 4H). It is noteworthy that during embryogenesis and early germination, *FRD3* is primarily expressed in the cell layers, in the embryo and the seed coat, that are facing the space surrounding the developing embryo. This observation, associated with the early phenotypic defect of germination of the *frd3* mutant, strongly suggests a role for citrate efflux in iron mobilization at this stage of development.

FRD3 Is Also Required at Reproductive Stages

As mentioned earlier, *frd3-7* plants are chlorotic and show reduced growth when cultivated in the greenhouse in long-day conditions (Figures 1B and 5A). Moreover, *frd3-7* plants were essentially sterile, with very few siliques formed (Figure 5B) and a seed yield as low as 2% of that of wild-type plants (Figures 5C and 5D). Irrigation of the plants with iron (500 μ M Fe-EDDHA) suppressed *frd3-7* chlorosis (Figures 5A and 5B). Iron treatment also rescued *frd3-7* silique development (Figure 5B) and increased

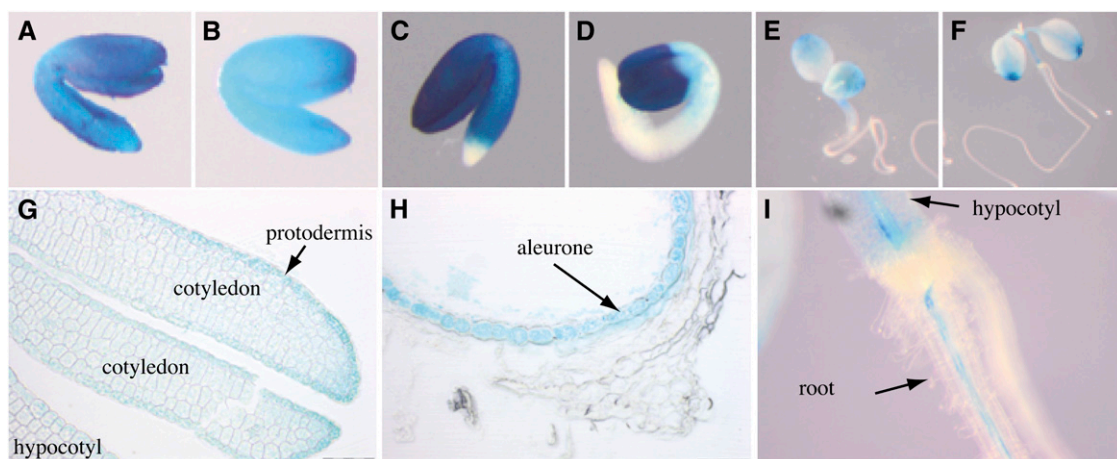


Figure 4. The *FRD3* Promoter Is Active during Embryogenesis and the Early Stages of Germination.

GUS histochemical staining of a representative proFRD3:GUS transgenic line.

(A) to (C) Dissected embryos from green siliques [(A) and (B)] or a dry seed (C).

(D) to (F) Seedling after 1 d (D), 3 d (E), or 5 d (F) of germination.

(G and H) Longitudinal section of a dry seed showing the embryo (G) or the seed envelope (H).

(I) Close-up image of the hypocotyl-root transition zone of a 5-d-old seedling. Scale bars = 50 μ m.

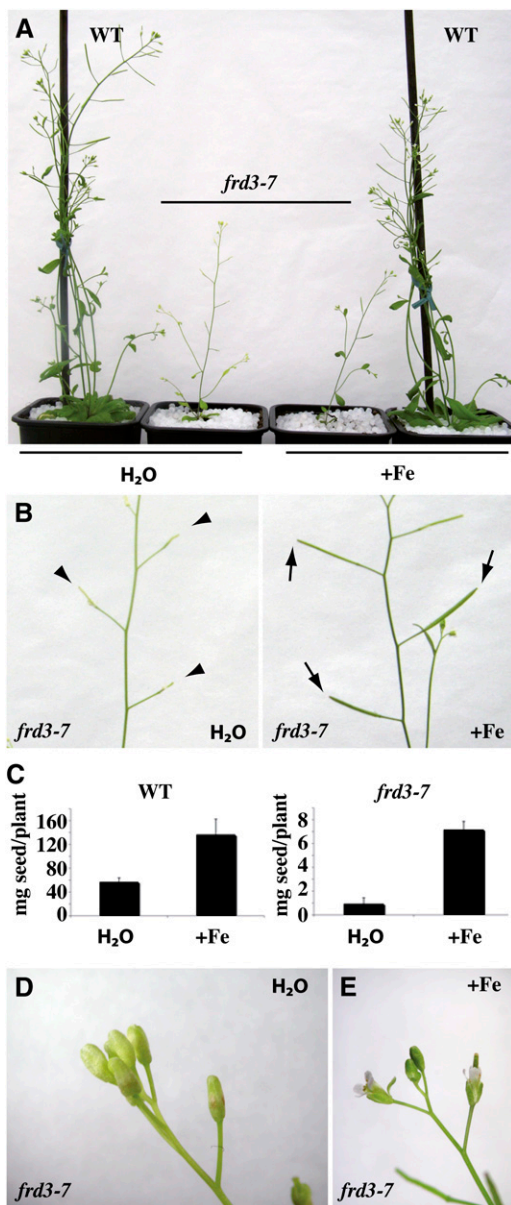


Figure 5. Phenotype of the *frd3* Mutant at the Reproductive Stage.

Wild-type and *frd3-7* plants were grown for 8 weeks in soil irrigated with water or 500 μ M FeEDDHA.

(A) to (E) Phenotypic defects of the *frd3-7* mutant and their rescue by iron. Chlorosis (A), production of altered siliques (B), reduced seed production (C), and absence of flower opening ([D] and [E]). Elongated (normal) and nonelongated (mutant) siliques are labeled with arrows and arrowheads, respectively (B). The graph (C) represents the mean of two independent experiments, each performed with six to eight plants. Error bars = SD. WT, wild type.

[See online article for color version of this figure.]

seed production by sevenfold in iron-supplied *frd3-7* plants compared with only 2.3-fold in wild-type plants (Figure 5C). Unlike chlorosis and sterility, however, the impaired growth of the mutant was not rescued by iron supplementation (Figure 5A). Instead, iron treatment exacerbated *frd3* dwarfism, suggesting that additional iron supply to the already iron-overloaded *frd3* mutant is toxic.

Inflorescences from water-irrigated *frd3-7* plants showed chlorotic flower buds that fail to open at stages 12 to 13 (Figure 5, compare D with E). As in rosette leaves of other *frd3* alleles (Delhaize, 1996; Rogers and Guerinot, 2002; Lahner et al., 2003), metal content in the inflorescence of the *frd3-7* mutant showed an increase in Mn and Co, as well as a decrease in iron (Table 1). When *frd3-7* plants were supplemented with iron, inflorescences regreened and flowers opened (Figure 5F). This suggests that the defect in flower development in *frd3-7* is caused by insufficient iron in the inflorescence. Altered fertility was also observed with two other *frd3* alleles, *frd3-1* and *frd3-6* (see Supplemental Figure 5 online), strongly supporting the view that FRD3 directly or indirectly plays a role in plant reproduction.

***Fr*3-7 Is Defective in Pollen Development**

To correlate *FRD3* expression pattern with the fertility abnormality of *frd3-7*, we investigated GUS activity in the flowers of Pro*FRD3*:GUS transgenic plants. *FRD3* promoter activity was found in the flower, restricted to the male gametophyte (Figures 6A and 6B). Cross-sections through the anther showed blue staining in the anther tissue and in the pollen grains (Figure 6C).

The finding that the *FRD3* promoter is strongly and specifically active in the male part of the flower prompted us to further characterize the impact of the loss of FRD3 on flower development and to examine pollen development in the *frd3-7* mutant. *frd3-7* flowers showed a defect in anther structure and lacked pollen grains at the anther surface compared with wild-type plants (Figures 7A and 7B). Microscopic analyses of the anther revealed that pollen grains are produced in *frd3* mutant plants but their viability is drastically reduced to 5% of the wild type (Table 2). Staining with Alexander's stain, which labels viable pollen in pink and dead pollen in blue, confirmed the presence of rare viable pollen grains in the mutant (Figures 7C and 7D). We next tested whether the *frd3-7* pollen phenotype is associated with low iron nutrition by irrigating the mutant with iron (500 μ M FeEDDHA, see Methods). The morphology of the pollen grains was examined by staining with periodic acid-Schiff-naphthol blue-black thin cross-sections of *frd3-7* anthers. Compared with water-irrigated plants that produced a majority of aborted pollen grains (Figure 7E, Table 2), the anthers of iron-treated plants developed 100% normal pollen grains (Figure 7F, Table 2), demonstrating that the phenotype of the mutant is caused by an alteration of iron nutrition of the pollen grains.

***frd3-7* Pollen Phenotype Results from a Gametophytic Mutation**

Because *FRD3* is expressed in pollen and in sporophytic tissues, including root and anther, and because all of the aerial parts of the *frd3* mutant are chlorotic, we asked whether the defect in pollen development is the consequence of the loss of *FRD3*

Table 1. Elemental Analysis of Wild-Type and *frd3-7* Inflorescences (mg/kg dry weight)

Genotype	Mn			Zn			Fe			Co		
	Mean	SD	Fold Change	Mean	SD	Fold Change	Mean	SD	Fold Change	Mean	SD	Fold Change
Wild type	115	22		215	105		55	12		0.52	0.07	
<i>frd3-7</i>	250	42	2.2**	205	11	0.95	39	5.3	0.71*	0.66	0.08	1.27*

Inductively coupled plasma-mass spectrometry measurement in inflorescences of wild-type and *frd3-7* plants grown in soil ($n = 4$). Significant differences between *frd3-7* and wild type are indicated as * $P < 0.05$ and ** $P < 0.01$, $n = 4$. One representative experiment ($n = 2$) is shown.

expression in the sporophyte, the gametophyte, or both. To that end, we took advantage of the fact that, as *frd3-7* is a recessive mutation, development of the *frd3-7/FRD3* heterozygous plant appears phenotypically wild type at the vegetative or reproductive stages. We sought to determine whether the 50% of haploid pollen grains that carry the *frd3* mutation in the *FRD3/frd3-7* background harbor a typical *frd3* developmental defect. Anthers from unopened flowers were sectioned at an early stage, i.e., prior to tapetum degeneration (Figure 8A), or at a mature stage when tapetal cells are gone (Figure 8B). At the early stage, pollen grains produced by *frd3-7/frd3-7* plants looked smaller than pollen grains from *FRD3/FRD3* anthers and had a collapsed cellular content (Figure 8G). Later on, the same pollen grains looked like debris of dead cells outlining the walls of the pollen sac (Figure 8H). In addition to the pollen defect, the tapetum of the *frd3-7/frd3-7* flowers contained noticeably expanded and vacuolated cells compared with wild-type tapetum (Figures 8A and 8G). When looking at *frd3-7/FRD3* anthers, we observed an equivalent number of both types of pollen grains (Table 2), wild-type, round shaped-pollen, and *frd3*-like collapsed pollen, despite the normal aspect of surrounding anther tissues (Figure 8E). This indicates that the developmental defect of *frd3* pollen is independent of the maternal tissues and primarily depends on the gametophytic expression of *FRD3*.

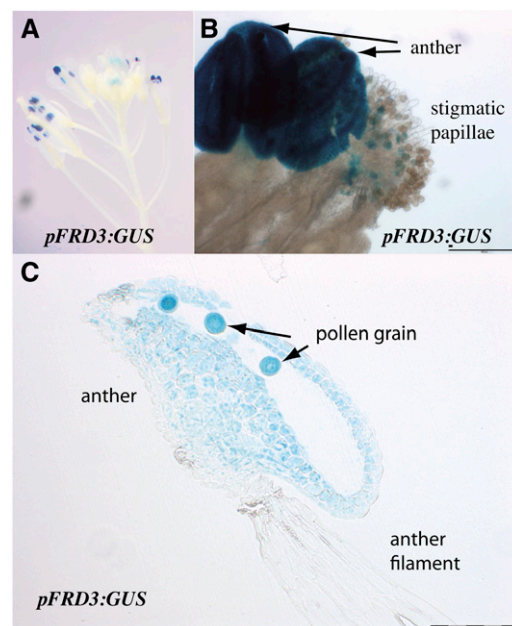
We next looked at the iron accumulation pattern in anthers of *FRD3/FRD3*, *frd3-7/FRD3* and *frd3-7/frd3-7* plants through Perl/DAB staining of thin flower sections (Figures 8C, 8F, and 8I). In the homozygous mutant anther, strong deposits of iron were observed in the anther locule that appeared to be located on the surface of the collapsed pollen grains (Figure 8I). No such iron accumulation was detected in the locule of wild-type anthers (Figure 8C). Consistently, the *frd3-7/FRD3* heterozygous anthers presented iron deposits that were restricted to the population of aborted pollen grains (Figure 8F). This result strongly suggests that the loss of *FRD3* in pollen prevents iron solubilization outside pollen and subsequent iron acquisition.

DISCUSSION

Previous studies had suggested a role for *FRD3*-mediated citrate efflux in the root-to-shoot translocation of iron in xylem vessels (Rogers and Guerinot, 2002; Green and Rogers, 2004; Durrett et al., 2007; Yokosho et al., 2009). Here, we report on important additional functions of *FRD3* and citrate in the mobilization of iron in seed and flower. We found strong expression of *FRD3* throughout the embryo, early in the maturation process, as well

as in the pollen grain. Consistently, loss-of-function mutations in *FRD3* alter germination in iron-limiting growth conditions and dramatically reduce fertility. We found that the sterility of *frd3* mutants is caused by a defect in pollen development, dependent on *FRD3* gametophytic expression, which correlates with a decrease of iron inside the aborted pollen grains and the presence of iron deposits on their surface. In addition, we have refined the location of iron in root and shoot of the *frd3* mutant and identified that leaf chlorosis is caused by retention of iron in the apoplast surrounding the vessels from the root up to leaf vasculature and by the resulting decrease of iron in its target organelles in leaf mesophyll cells.

In *frd3* roots, iron deposits were observed specifically in the apoplastic zone, whereas symplastic iron remained unchanged, which supports the current view that citrate efflux in the apoplast is necessary to solubilize iron in the extracellular space. Iron accumulation is restricted to the stele, i.e., the region contained

**Figure 6.** *FRD3* Promoter Activity in Flower.

GUS histochemical staining of an inflorescence of a representative *pFRD3:GUS* transgenic line.

(A) Inflorescence.

(B) Anther and stigmatic papillae.

(C) Longitudinal section of a stamen. Scale bars = 100 μm .

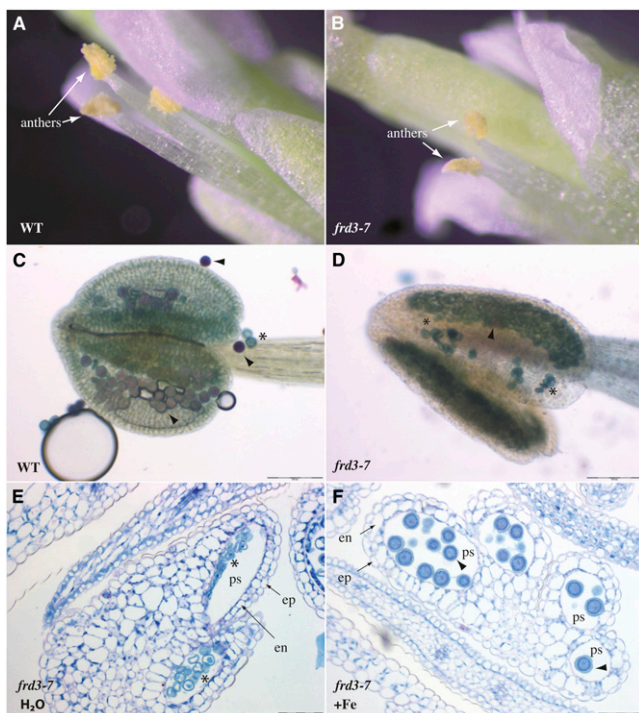


Figure 7. Pollen Development Is Impaired in *frd3-7*.

(A) and (B) Detailed view of a wild-type (WT; [A]) and an *frd3-7* flower (B), highlighting the morphological difference of the *frd3-7* anthers.

(C) and (D) Pollen viability assay in wild-type (C) or *frd3-7* anthers (D) using the Alexander's stain. Viable and dead pollen grains are stained in pink and blue, respectively.

(E) and (F) Periodic acid-Schiff-naphthol blue-black-stained cross sections of mature flowers collected from *frd3-7* plants irrigated (F) or not (E) with 0.5 μ M FeEDDHA. Arrowhead, normal pollen; asterisk, abnormal pollen; ep, epidermis; en, endothecium; ps, pollen sac. Scale bars = 50 μ m in (E) and (F) and 100 μ m in (C) and (D).

within the boundaries of the casparian strip, which therefore acts as a tight barrier for iron circulation. Consequently, to penetrate into the stele, iron must take a symplastic route. Candidates for iron entry in the symplast of the external layers are primarily IRT1 in the epidermis and cortex (Vert et al., 2002) and Natural Resistance-Associated Macrophage Protein1 in the endodermis (Cailliatte et al., 2010). A second consequence is that cells of the stele must have iron efflux activity to provide the apoplastic compartment with iron. Ferroportin 1 (FPN1) is an iron and cobalt efflux transporter that is expressed in the root central cylinder where it might participate in metal loading of the xylem sap (Morrissey et al., 2009). Therefore, we reasoned that if FRD3 and FPN1 act synchronously to efflux citrate and iron, respectively, knocking out *FPN1* in the *frd3* background would prevent accumulation of iron in the stele and rescue *frd3* phenotype. However, Perls staining indicated that the deposition of iron in the root of the *frd3 fpn1* double mutant was similar to that in the *frd3* single mutant (see Supplemental Figure 6 online).

At the vegetative stage, we observed high amounts of iron deposited in the vascular tissues not only of roots, but also of

other organs such as hypocotyl and leaf, despite the absence of expression of *FRD3* in these tissues. In the hypocotyl, iron was found to accumulate mostly around the xylem. In leaf vasculature too, a dramatic iron accumulation was observed in xylem. Concomitant with the increase of iron in leaf xylem, mesophyll and xylem parenchyma cells showed a loss of the intracellular iron. This was already suggested by the reduction of iron content in *frd3* leaf protoplasts (Green and Rogers, 2004). However, iron imaging provides the final proof that in *frd3*, iron does not enter the symplast of leaf cells, which explains the chlorotic symptoms and constitutive root iron uptake activity of the *frd3* mutant. Moreover, iron accumulation in *frd3* leaf is concentrated in the vascular tissue, while no iron diffusion was observed around mesophyll cells. This result indicates that Fe-citrate in leaf is primarily required for xylem unloading and/or for loading of iron in the cells adjacent to xylem vessels. If Fe-citrate provides iron directly to mesophyll cells, one would expect to observe, in *frd3*, a local accumulation of iron in the apoplast surrounding these cells. The fact that iron accumulates specifically in xylem, but not around adjacent cells, indicates that xylem parenchyma forms an efficient barrier to apoplastic iron circulation in leaf tissues. It is an interesting question as to whether Fe-citrate enters directly into these xylem-associated cells via an unidentified transport system or whether it donates iron to a ferric-chelate reductase that provides Fe^{2+} to a leaf-expressed ZRT-IRT LIKE PROTEIN-like family transporter (Figure 9).

In *frd3*, iron reaches the aerial organs, which suggests that citrate efflux is not necessary for root-to-shoot translocation of iron in xylem sap. In the absence of citrate in the apoplast, free Fe^{3+} ions likely bind components of the cell wall in the root central cylinder. Because iron uptake is very high in *frd3*, iron accumulating in the vasculature of the plant may slowly saturate the binding sites in the cell walls, prompting iron to move along the path and gradually reach aerial tissues. Alternately, organic acids, such as malate, that are present in the sap could in theory chelate Fe^{3+} and promote its translocation to the shoot. Whether such complexes are too inefficient to donate iron to leaf cells, hence, leading to the *frd3* chlorotic phenotype, remains an open question. It is worth mentioning that we have not measured any increase of this organic acid in *frd3* xylem exudates that could compensate for the decrease of citrate (see Supplemental Figure 2 online).

Table 2. Pollen Viability in the *frd3* Mutant

<i>frd3-7</i> genotype	-Fe		+Fe	
	Normal Pollen (%)	Abnormal Pollen (%)	Normal Pollen (%)	Abnormal Pollen (%)
+/+	100	0	100	0
-/-	5	95	100	0
+/-	52	48	n.d.	n.d.

Percentage of normal and abnormal pollen estimated in naphthol blue black-stained sections obtained from five to 10 flowers of two individual plants from two independent experiments. Plants were irrigated with water (-Fe) or 0.5 mM FeEDDHA (+Fe) to rescue pollen development. n.d., not defined.

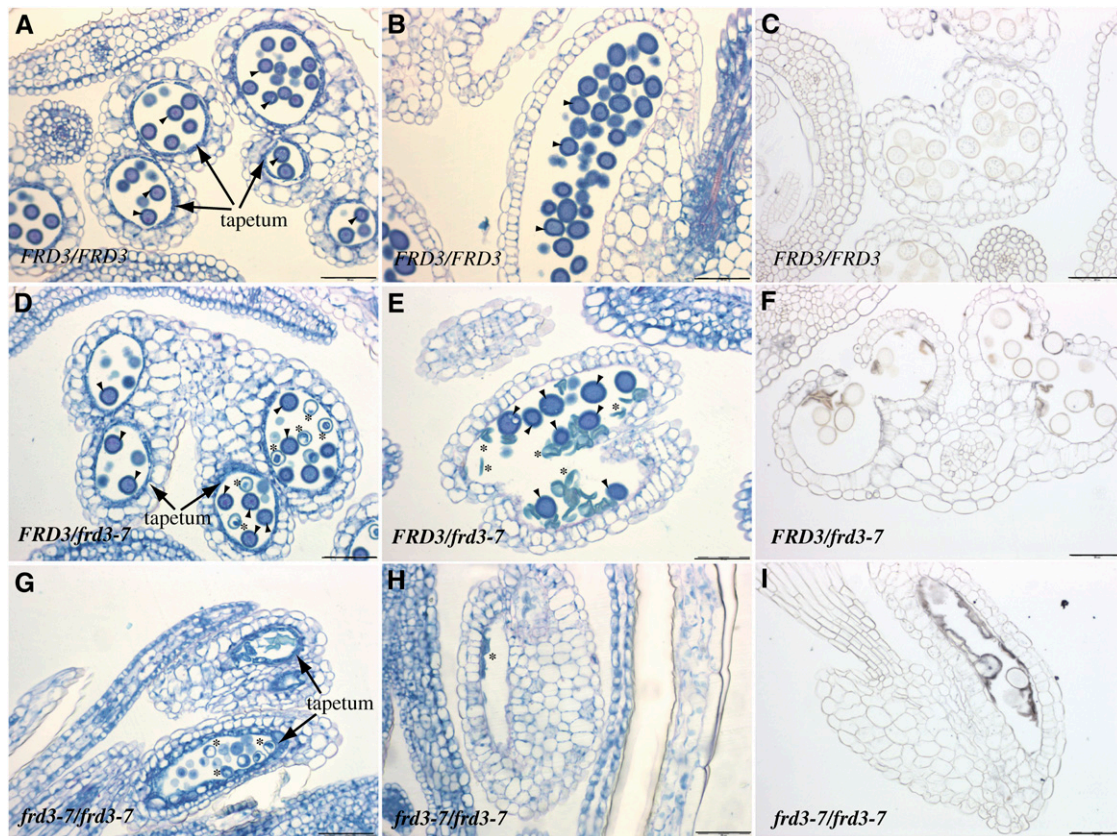


Figure 8. The *frd3* Mutation Acts Gametophytically to Alter Pollen Development.

(A) to (I) Histological sections of flowers from wild-type *FRD3/FRD3* [(A) to (C)], heterozygous *FRD3/frd3-7* [(D) to (F)], or homozygous mutant *frd3-7/frd3-7* plants [(G) and (H)] stained with periodic acid-Schiff-naphthol blue-black [(A), (B), (D), (E), (G), and (H)] or with Perls/DAB [(C), (F), and (I)].

(A), (D), and (G) Immature anther containing pollen at the two-cell stage.

(B), (C), (E), (F), (H), and (I) Mature anther containing trinucleated pollen before dehiscence. Arrowhead, normal pollen; asterisk, abnormal pollen. Scale bars = 50 μm .

Although iron supply rescues germination, chlorosis, and fertility of *frd3*, it does not rescue its growth (Figure 5). It is possible that in addition to being iron deficient, the *frd3* mutant suffers from citrate shortage, thereby potentially affecting the numerous metabolic processes in which citrate takes part, including cellular respiration, fatty acid synthesis, and glycolysis. Alternately, iron supply to the *frd3* mutant, which already accumulates high levels of iron in the vasculature, might become toxic for the plant and inhibit its growth. This hypothesis is supported by (1) the strong ferritin accumulation in *frd3* roots (Green and Rogers, 2004) and (2) the pronounced inhibition of *frd3* growth upon iron treatment (Figure 6A).

In addition to the well-known expression of *FRD3* in the root, we found strong *FRD3* promoter activity in seeds—throughout the embryo, particularly in the protodermis of the cotyledons and hypocotyl-root axis, and in the aleurone layer facing the embryo in the seed envelope. During the first 3 d of germination, growth of *frd3* was retarded and its cotyledons were chlorotic in conditions of iron deficiency, a defect that was rescued by iron or citrate supplementation (Figure 3). This strongly suggests that citrate excretion by *FRD3* also plays a role in the embryonic iron

nutrition during embryogenesis. Because the root is not competent at this stage to take up iron, a possibility exists that cells of the embryonic surface, including cotyledons and hypocotyl, have their own machinery to take up iron that depends on iron availability in the surrounding nutritive fluid. Thus, solubilization of iron by citrate around the embryo could be a prerequisite for direct iron uptake by embryo cells. However, if this is the case, this process is not important for embryo development because we have not observed any morphological alteration of *frd3* embryos. It could represent the initial step in the building of the vacuolar iron stores in the endodermis of the embryo (Roschztardt et al., 2009); however, the characteristic pattern of embryonic iron was not modified in *frd3* embryos (Figure 3). Because loss of *FRD3* affects seed germination, its role could be, via the release of citrate from the seed envelope and the embryo, to mobilize putative iron apoplastic stores of the embryo prior to the onset of IRT1 synthesis that occurs 3 d postgermination (Lanquar et al., 2005).

Our analysis shows that *FRD3* is required for the development of the male gametophyte and highlights a role for citrate in the process of iron delivery to the pollen grains. *frd3-7* flowers

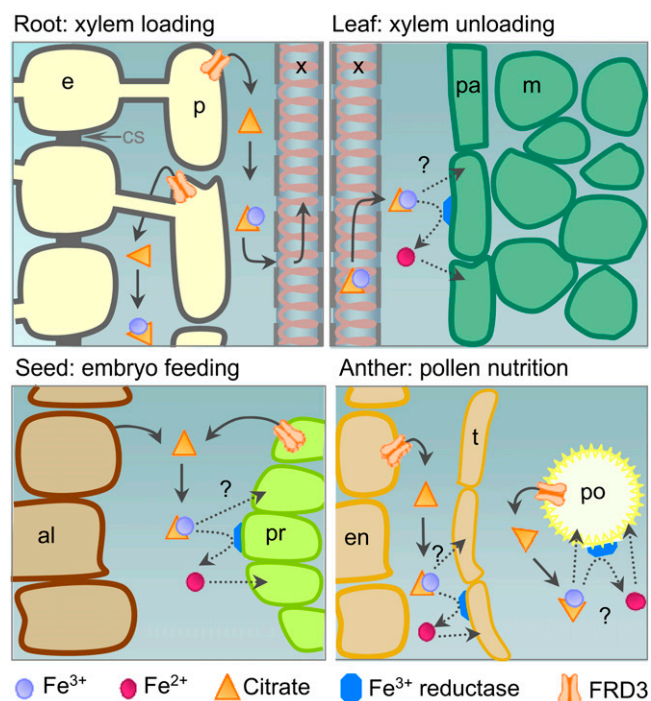


Figure 9. Model for the Role of FRD3 in Iron Nutrition between Symplastically Disconnected Tissues.

Schematic representation of the proposed role of FRD3 in the different organs at different developmental stages. Top left, FRD3 in the root pericycle is required for solubilization of iron in the apoplast surrounding the stele cells and for proper loading of iron in the xylem sap. This citrate efflux activity might function in coordination with an iron efflux activity from endodermis or pericycle. Top right, Although not produced in leaves, citrate released by FRD3 in the central apoplast of the root is necessary for proper iron loading in the limb cells of the leaf. Bottom left, In the seed, where *FRD3* expression is high in the embryo, particularly in the protodermis, and in the aleurone layer of the seed envelope, FRD3 might function to release citrate in the space separating the embryo and the envelope to provide available iron to feed the embryo. Bottom right, in the anther, the pollen grain depends on the pollen expression of *FRD3* for its maturation and on the sporophytic expression of *FRD3* for optimal iron loading, indicating that citrate efflux in the pollen sac is likely to increase iron solubility and to promote, directly or indirectly, iron acquisition by the pollen grain. In addition, tapetum morphogenesis requires a functional FRD3. In the three latter organs, seed, anther, and leaf, subsequent entry of iron in the sink tissue could occur as an Fe(III)-citrate complex by an as yet unidentified transporter or, after reduction into Fe(II), through a divalent metal transporter of the ZRT-IRT LIKE PROTEIN or Natural Resistance-Associated Macrophage Protein1 families. Because the four above-described situations share the common feature that iron transport from source to sink tissues involves an apoplastic step, we propose that FRD3-mediated citrate efflux is a prerequisite for iron traffic between symplastically disconnected tissues. al, aleurone; e, endodermis; en, endothecium; m, mesophyll cell; p, pericycle; pa, parenchyma; po, pollen grain; pr, protodermis; t, tapetum; x, xylem.

[See online article for color version of this figure.]

produce nonviable aborted pollen grains, unless the plant is irrigated with a solution of iron. The fact that iron supplementation fully rescues *frd3* pollen development strongly suggests that iron nutrition of pollen is impaired in the mutant. In addition, it might explain why previous studies have failed to see a fertility defect in *frd3* mutant alleles, as iron availability varies greatly according to the soil or culture medium used. Despite our rather iron-limiting growth conditions, we have found that the *frd3* mutation is not fully penetrant. Indeed, *frd3* plants do set a few seeds (Figure 5C) and viable pollen grains are occasionally observed in the mutant anthers (Figures 7D and 8I).

Despite the *FRD3* gene being expressed in the sporophytic and the gametophytic tissues of the anther, we have demonstrated that the *frd3* mutation acts gametophytically to affect pollen development. Indeed, heterozygous *FRD3/frd3-7* plants harboring phenotypically wild-type inflorescence and anthers display ~50% of aborted pollen grains (Figure 8F, Table 1). Histochemical staining of iron revealed the presence of strong deposits at the surface of the aborted pollen grains in heterozygous and homozygous mutant anthers. It strongly suggests that in the absence of citrate efflux from the pollen grain, iron precipitates at the surface, thereby preventing its uptake by the pollen. Similar to the situation in embryo and leaf vasculature, whether iron enters pollen as Fe-citrate or whether it is solubilized by citrate prior to its reduction and transport as Fe²⁺ remains an open question.

The role of sporophytic FRD3 in anther and pollen development appears significant as well. The tapetum layer that outlines the pollen sac shows clear cytological alterations as cells exhibit drastically enlarged vacuoles (Figure 8G). Thus, FRD3 is also required for normal development of anther tissue and, in particular, the tapetum. Furthermore, iron content inside the pollen grain, which is clearly visible in wild-type plants, is hardly detectable in the viable pollen grains from heterozygous or homozygous *frd3* plants (Figures 8C and 8F). This suggests that the presence of FRD3 in the sporophytic anther tissue contributes to iron nutrition of the pollen grains.

If citrate is released into the anther lumen by tapetal cells and pollen grains, why does pollen from heterozygous plants fail to develop, i.e., why does the sporophytic activity fail to rescue the loss of gametophytic activity? The total amount of citrate released in the pollen sac of the heterozygote might be insufficient to support pollen growth. Indeed, wild-type pollen grains from *FRD3/frd3-7* plants contain less iron than do pollen grains from *FRD3/FRD3* plants (Figure 8, compare F to C). Consistent with the finding that the pollen developmental defect of *frd3* is mostly gametophytic, aborted pollen grains from the heterozygote show iron accumulated on their surface, which suggests that citrate efflux activity is most efficient when present locally around the pollen grain.

Citrate and nicotianamine (NA) are the two well-known iron ligands in plant tissues. Thanks to the existence of the natural NA-less tomato mutant *chloronerva*, the importance of NA in iron nutrition of developing tissues and in fertility has been shown. As opposed to NA, the precise contribution of citrate in plant iron homeostasis has been difficult to investigate because citrate is a multifunctional metabolite whose depletion would result in pleiotropic effects. Our study, in which the effect of FRD3 suppression

has been scrutinized throughout the development of the plant, has provided valuable insights into the iron nutrition pathway during embryogenesis and microsporogenesis and has revealed the decisive contribution of citrate to these processes.

Deciphering the function of FRD3 at the whole plant level has led us to the interesting finding that FRD3 mediated-citrate efflux always occurs toward an extracellular space separating two tissues deprived of symplastic connections. It is the case between pericycle and xylem, as suggested in previous studies, but also between the embryo and the seed envelope, and between pollen and surrounding anther tissues (Figure 9). Therefore, we propose a model in which iron nutrition of such disconnected tissues depends on iron solubilization by citrate outside the cells. From our data emerges a new paradigm in which iron chelation by citrate is a prerequisite step for iron nutrition in extracellular fluids. Recently, complexation of iron by citrate has been proposed as an important event in the blood-to-brain circulation of iron (Moos et al., 2007), thus supporting the view that our model might be generalized to extracellular traffic of iron in eukaryotes.

METHODS

Plant Material and Growth Conditions

Except for *frd3-1*, which is in the Columbia (Col)-1 ecotype, all the genotypes used are in the Col-0 ecotype. Seeds of the *frd3-7* mutant (SALK_122235) were obtained from the ABRC. The *frd3-1* allele, obtained in the *glabra1* background (Rogers and Guerinot, 2002), was kindly provided by Elizabeth Rogers (U.S. Department of Agriculture/Agricultural Research Service). The *frd3-1 fpn1-1* double mutant (Morrissey et al., 2009) was obtained from Mary Lou Guerinot (Dartmouth College). The *frd3-6* mutant was obtained from a forward genetic screen of EMS-mutagenized Col-0 plants carrying the *ProIRT1:LUCIFERASE* transgene (see Supplemental Figure 1 online).

For seed germination experiments, seeds were surface-sterilized and sown on 0.5× Murashige and Skoog medium with Suc, containing (+Fe) or not (−Fe), 50 μM Fe-EDTA and, when indicated in the legend, 3 mM sodium citrate (care was taken to adjust the pH of the medium to 5.7 after addition of sodium citrate) during 3.5 d at 21°C with a 16-h/8-h light/dark cycle. Plants cultivated in the greenhouse were grown on soil (Humin substrate N2 Neuhaus; Klasmann-Deilmann) at 23°C with a sunlight intensity limited to 300 μmol.m^{−2}.s^{−1} and 16-h light/8-h light/dark cycles.

frd3-7 Molecular Characterization

frd3-7 plants were genotyped by PCR using a T-DNA left border-specific primer (LBb1 5'GCGTGGACCGCTTGCTGCAACT3') and *FRD3* gene-specific primers (5'CCATTGCCATGTCATTCTC3' and 5'ACTAAGT-CCTAGGAAGATGAAGAG3'). Segregation on kanamycin revealed a 3:1 ratio characteristic of a single T-DNA insertion. Sequencing of the T-DNA flanking sequences indicated that the eighth exon of *FRD3* contains a complex insertion of two or more T-DNA copies (Figure 1C).

ProFRD3:GUS Transgenic Lines

The *FRD3* promoter fragment was amplified with the following primers: 5'ACGCGTGCACATGAAAAGGGGAAGTGGCAATG3' and 5'CATGCCA-TGGATCTTTTCTCTGTAAGT3', which contain the *Sall* and *NotI* restriction sites, respectively. The digested fragment was first cloned in the pRITA vector in translational fusion with the *uidA* gene encoding the GUS. The *proFRD3:GUS* cassette was then subcloned into the *NotI* site of

the binary vector pART27 (Gleave, 1992). Twelve independent transgenic *Arabidopsis thaliana* lines were obtained following floral dip transformation (Clough and Bent, 1998).

Metal Content

Samples were dried for 2 d at 80°C. For mineralization, tissues were digested completely (1–3 h) in 70% HNO₃ at 120°C. In seeds, iron content was determined as described in Lobreaux and Briat (1991). Metal measurement in the inflorescences was performed by inductively coupled plasma-mass spectrometry.

Microscopy Analyses

Histochemical GUS staining was performed as described in Elorza et al. (2004) using 1 mM 5-bromo-4-chloro-3-indolyl-β-D-glucuronide as a substrate (Jefferson et al., 1987). Flowers were fixed by 30 min of vacuum infiltration followed by 15 h of soaking in a solution containing 2% (w/v) paraformaldehyde, 1% (v/v) glutaraldehyde, and 1% (w/v) caffeine in 100 mM phosphate buffer (pH 7). Flowers were then dehydrated in successive baths of 50%, 70%, 90%, 95%, and 100% ethanol, butanol/ethanol 1:1 (v/v), and 100% butanol, and were embedded in the Technovit 7100 resin (Kulzer) according to the manufacturer's instructions. Thin sections (3 μm) were cut (Roschztardt et al., 2009) and stained with Periodic acid-Schiff's reagent (Merck) and naphtol blue black (Sigma) to stain carbohydrates and proteins, respectively. After hydrolysis with periodic acid (1% in distilled water) for 5 min, the sections were rinsed with distilled water. In the dark, sections were stained with Schiff's reagent for 10 min and were then rinsed with a solution containing 0.25% sodium metabisulfite and 0.05N HCl for 2 min. Sections were rinsed with distilled water, stained with naphtol blue black for 15 s (1 g of naphtol blue black, 7 mL of acetic acid, and 100 mL of distilled water), and rinsed with distilled water again. The samples were regressed with acetic acid at 7% and air-dried.

For histochemical iron localization, iron was stained in embryos and in tissue sections using the Perls (*fpn1 frd3* mutant) or the Perls/DAB protocol (all the other experiments) following the method described by Roschztardt et al. (2009).

Vital staining of the pollen grains was performed by incubating anthers in Alexander's stain for 15 min (Johnson-Brousseau and McCormick, 2004).

Accession Numbers

Sequence data from this article can be found in Arabidopsis Genome Initiative or GenBank/EMBL databases under the following accession numbers: FRD3, At3g08040; FRO2, At1g01580; and IRT1, At4g19690.

Supplemental Data

The following materials are available in the online version of this article.

Supplemental Figure 1. Isolation and Characterization of Two Novel *frd3* Alleles.

Supplemental Figure 2. Metabolic and Elemental Analysis of *frd3-7* Xylem Exudates.

Supplemental Figure 3. Germination Phenotype of Two Independent *frd3* Alleles.

Supplemental Figure 4. Expression Analysis of *FRD3* in the Main Organs.

Supplemental Figure 5. Sterility Phenotype of Different *frd3* Mutant Alleles.

Supplemental Figure 6. *FPN1* Mutation Does Not Prevent Iron Accumulation in the *frd3* Root.

ACKNOWLEDGMENTS

We thank Elizabeth Rogers (U.S. Department of Agriculture/Agricultural Research Service) for sending the *frd3-1* seeds, Mary Lou Guerinot (Dartmouth College) for the gift of the *frd3 fpn1* mutant line, Marc Lepetit (Biochimie et Physiologie Moléculaire des Plantes) for his advice on forward genetic screening, Brigitte Touraine for her help with the high-performance ionic chromatography experiments, and Stéphane Mari for helpful discussions. This work was funded by the Agence Nationale de Recherche programs CIDS 06-BLAN-0106 and DISTRIMET 07-BLAN-0110. H.R. was supported by the DISTRIMET 07-BLAN-0110 program and M.S. was supported by the French Ministry of Education and Research.

AUTHOR CONTRIBUTIONS

H.R. and M.S.-A. did the research and analyzed data; C.C., J-F.B., and G.V. designed the research; and C.C. wrote the article.

Received June 8, 2011; revised June 8, 2011; accepted June 21, 2011; published July 8, 2011.

REFERENCES

- Brown, J.C.** (1966). Fe and Ca uptake as related to root-sap and stem-exudate citrate in soybeans. *Physiol. Plant.* **19**: 968–976.
- Cailliatte, R., Schikora, A., Briat, J.F., Mari, S., and Curie, C.** (2010). High-affinity manganese uptake by the metal transporter NRAMP1 is essential for *Arabidopsis* growth in low manganese conditions. *Plant Cell* **22**: 904–917.
- Clough, S.J., and Bent, A.F.** (1998). Floral dip: A simplified method for Agrobacterium-mediated transformation of *Arabidopsis thaliana*. *Plant J.* **16**: 735–743.
- Colangelo, E.P., and Guerinot, M.L.** (2004). The essential basic helix-loop-helix protein FIT1 is required for the iron deficiency response. *Plant Cell* **16**: 3400–3412.
- Connolly, E.L., Fett, J.P., and Guerinot, M.L.** (2002). Expression of the IRT1 metal transporter is controlled by metals at the levels of transcript and protein accumulation. *Plant Cell* **14**: 1347–1357.
- Debeaujon, I., Peeters, A.J., Léon-Kloosterziel, K.M., and Koomneef, M.** (2001). The TRANSPARENT TESTA12 gene of *Arabidopsis* encodes a multidrug secondary transporter-like protein required for flavonoid sequestration in vacuoles of the seed coat endothelium. *Plant Cell* **13**: 853–871.
- Delhaize, E.** (1996). A metal-accumulator mutant of *Arabidopsis thaliana*. *Plant Physiol.* **111**: 849–855.
- Durrett, T.P., Gassmann, W., and Rogers, E.E.** (2007). The FRD3-mediated efflux of citrate into the root vasculature is necessary for efficient iron translocation. *Plant Physiol.* **144**: 197–205.
- Eide, D., Broderius, M., Fett, J., and Guerinot, M.L.** (1996). A novel iron-regulated metal transporter from plants identified by functional expression in yeast. *Proc. Natl. Acad. Sci. USA* **93**: 5624–5628.
- Elorza, A., León, G., Gómez, I., Mouras, A., Holuigue, L., Araya, A., and Jordana, X.** (2004). Nuclear SDH2-1 and SDH2-2 genes, encoding the iron-sulfur subunit of mitochondrial complex II in *Arabidopsis*, have distinct cell-specific expression patterns and promoter activities. *Plant Physiol.* **136**: 4072–4087.
- Furukawa, J., Yamaji, N., Wang, H., Mitani, N., Murata, Y., Sato, K., Katsuhara, M., Takeda, K., and Ma, J.F.** (2007). An aluminum-activated citrate transporter in barley. *Plant Cell Physiol.* **48**: 1081–1091.
- Gleave, A.P.** (1992). A versatile binary vector system with a T-DNA organisational structure conducive to efficient integration of cloned DNA into the plant genome. *Plant Mol. Biol.* **20**: 1203–1207.
- Gomez, C., Terrier, N., Torregrosa, L., Vialet, S., Fournier-Level, A., Verriès, C., Souquet, J.M., Mazauric, J.P., Klein, M., Cheynier, V., and Ageorges, A.** (2009). Grapevine MATE-type proteins act as vacuolar H⁺-dependent acylated anthocyanin transporters. *Plant Physiol.* **150**: 402–415.
- Green, L.S., and Rogers, E.E.** (2004). FRD3 controls iron localization in *Arabidopsis*. *Plant Physiol.* **136**: 2523–2531.
- Henriques, R., Jásik, J., Klein, M., Martinoia, E., Feller, U., Schell, J., Pais, M.S., and Koncz, C.** (2002). Knock-out of *Arabidopsis* metal transporter gene IRT1 results in iron deficiency accompanied by cell differentiation defects. *Plant Mol. Biol.* **50**: 587–597.
- Jakoby, M., Wang, H.Y., Reidt, W., Weisshaar, B., and Bauer, P.** (2004). FRU (BHLH029) is required for induction of iron mobilization genes in *Arabidopsis thaliana*. *FEBS Lett.* **577**: 528–534.
- Jefferson, R.A., Kavanagh, T.A., and Bevan, M.W.** (1987). GUS fusions: beta-Glucuronidase as a sensitive and versatile gene fusion marker in higher plants. *EMBO J.* **6**: 3901–3907.
- Johnson-Brousseau, S.A., and McCormick, S.** (2004). A compendium of methods useful for characterizing *Arabidopsis* pollen mutants and gametophytically expressed genes. *Plant J.* **39**: 761–775.
- Lahner, B., Gong, J., Mahmoudian, M., Smith, E.L., Abid, K.B., Rogers, E.E., Guerinot, M.L., Harper, J.F., Ward, J.M., McIntyre, L., Schroeder, J.I., and Salt, D.E.** (2003). Genomic scale profiling of nutrient and trace elements in *Arabidopsis thaliana*. *Nat. Biotechnol.* **21**: 1215–1221.
- Lanquar, V., Lelièvre, F., Bolte, S., Hamès, C., Alcon, C., Neumann, D., Vansuyt, G., Curie, C., Schröder, A., Krämer, U., Barbier-Brygoo, H., and Thomine, S.** (2005). Mobilization of vacuolar iron by AtNRAMP3 and AtNRAMP4 is essential for seed germination on low iron. *EMBO J.* **24**: 4041–4051.
- Li, L., He, Z., Pandey, G.K., Tsuchiya, T., and Luan, S.** (2002). Functional cloning and characterization of a plant efflux carrier for multidrug and heavy metal detoxification. *J. Biol. Chem.* **277**: 5360–5368.
- Liu, J.P., Magalhaes, J.V., Shaff, J., and Kochian, L.V.** (2009). Aluminum-activated citrate and malate transporters from the MATE and ALMT families function independently to confer *Arabidopsis* aluminum tolerance. *Plant J.* **57**: 389–399.
- Lobreaux, S., and Briat, J.F.** (1991). Ferritin accumulation and degradation in different organs of pea (*Pisum sativum*) during development. *Biochem. J.* **274**: 601–606.
- López-Millán, A.F., Morales, F., Abadía, A., and Abadía, J.** (2000). Effects of iron deficiency on the composition of the leaf apoplastic fluid and xylem sap in sugar beet. Implications for iron and carbon transport. *Plant Physiol.* **124**: 873–884.
- Marinova, K., Pourcel, L., Weder, B., Schwarz, M., Barron, D., Routaboul, J.M., Debeaujon, I., and Klein, M.** (2007). The *Arabidopsis* MATE transporter TT12 acts as a vacuolar flavonoid/H⁺-antiporter active in proanthocyanidin-accumulating cells of the seed coat. *Plant Cell* **19**: 2023–2038.
- Maron, L.G., Piñeros, M.A., Guimarães, C.T., Magalhaes, J.V., Pleiman, J.K., Mao, C.Z., Shaff, J., Belicuas, S.N.J., and Kochian, L.V.** (2010). Two functionally distinct members of the MATE (multi-drug and toxic compound extrusion) family of transporters potentially underlie two major aluminum tolerance QTLs in maize. *Plant J.* **61**: 728–740.

- Momono, K., Yoshida, K., Mano, S., Takahashi, H., Nakamori, C., Shoji, K., Nitta, A., and Nishimura, M.** (2009). A vacuolar iron transporter in tulip, TgVit1, is responsible for blue coloration in petal cells through iron accumulation. *Plant J.* **59**: 437–447.
- Moos, T., Rosengren Nielsen, T., Skjærtinge, T., and Morgan, E.H.** (2007). Iron trafficking inside the brain. *J. Neurochem.* **103**: 1730–1740.
- Morrissey, J., Baxter, I.R., Lee, J., Li, L.T., Lahner, B., Grotz, N., Kaplan, J., Salt, D.E., and Guerinot, M.L.** (2009). The ferroportin metal efflux proteins function in iron and cobalt homeostasis in *Arabidopsis*. *Plant Cell* **21**: 3326–3338.
- Omote, H., Hiasa, M., Matsumoto, T., Otsuka, M., and Moriyama, Y.** (2006). The MATE proteins as fundamental transporters of metabolic and xenobiotic organic cations. *Trends Pharmacol. Sci.* **27**: 587–593.
- Rellán-Alvarez, R., Giner-Martínez-Sierra, J., Orduna, J., Orera, I., Rodríguez-Castrillón, J.A., García-Alonso, J.I., Abadía, J., and Álvarez-Fernández, A.** (2010). Identification of a tri-iron(III), tri-citrate complex in the xylem sap of iron-deficient tomato resupplied with iron: New insights into plant iron long-distance transport. *Plant Cell Physiol.* **51**: 91–102.
- Robinson, N.J., Procter, C.M., Connolly, E.L., and Guerinot, M.L.** (1999). A ferric-chelate reductase for iron uptake from soils. *Nature* **397**: 694–697.
- Rogers, E.E., and Guerinot, M.L.** (2002). FRD3, a member of the multidrug and toxin efflux family, controls iron deficiency responses in *Arabidopsis*. *Plant Cell* **14**: 1787–1799.
- Roschttardt, H., Conéjéro, G., Curie, C., and Mari, S.** (2009). Identification of the endodermal vacuole as the iron storage compartment in the *Arabidopsis* embryo. *Plant Physiol.* **151**: 1329–1338.
- Santi, S., and Schmidt, W.** (2009). Dissecting iron deficiency-induced proton extrusion in *Arabidopsis* roots. *New Phytol.* **183**: 1072–1084.
- Schmidt, W.** (1999). Mechanisms and regulation of reduction-based iron uptake in plants. *New Phytol.* **141**: 1–26.
- Takahashi, M., Terada, Y., Nakai, I., Nakanishi, H., Yoshimura, E., Mori, S., and Nishizawa, N.K.** (2003). Role of nicotianamine in the intracellular delivery of metals and plant reproductive development. *Plant Cell* **15**: 1263–1280.
- Varotto, C., Maiwald, D., Pesaresi, P., Jahns, P., Salamini, F., and Leister, D.** (2002). The metal ion transporter IRT1 is necessary for iron homeostasis and efficient photosynthesis in *Arabidopsis thaliana*. *Plant J.* **31**: 589–599.
- Vert, G., Grotz, N., Dédaldéchamp, F., Gaymard, F., Guerinot, M.L., Briat, J.F., and Curie, C.** (2002). IRT1, an *Arabidopsis* transporter essential for iron uptake from the soil and for plant growth. *Plant Cell* **14**: 1223–1233.
- Vert, G.A., Briat, J.F., and Curie, C.** (2003). Dual regulation of the *Arabidopsis* high-affinity root iron uptake system by local and long-distance signals. *Plant Physiol.* **132**: 796–804.
- Yazaki, K.** (2005). Transporters of secondary metabolites. *Curr. Opin. Plant Biol.* **8**: 301–307.
- Yokosho, K., Yamaji, N., Ueno, D., Mitani, N., and Ma, J.F.** (2009). OsFRDL1 is a citrate transporter required for efficient translocation of iron in rice. *Plant Physiol.* **149**: 297–305.
- Yuan, Y.X., Zhang, J., Wang, D.W., and Ling, H.Q.** (2005). AtbHLH29 of *Arabidopsis thaliana* is a functional ortholog of tomato FER involved in controlling iron acquisition in strategy I plants. *Cell Res.* **15**: 613–621.
- Zhao, J., and Dixon, R.A.** (2009). MATE transporters facilitate vacuolar uptake of epicatechin 3'-O-glucoside for proanthocyanidin biosynthesis in *Medicago truncatula* and *Arabidopsis*. *Plant Cell* **21**: 2323–2340.